

Cite this: DOI: 00.0000/xxxxxxxxxx

Potential energy surface study of $X@Si_{32}X_{44}^-$ ($X=Cl, Br$) clusters to decipher the stabilization process of Si_{20} fullerene

Deb Sankar De,^{*a} Santanu Saha,^b and Stefan Goedecker^a

Received Date

Accepted Date

DOI: 00.0000/xxxxxxxxxx

Efforts toward stabilization of the Si_{20} fullerene through different schemes have failed despite several theoretical predictions. However, recently Tillmann *et al.* succeeded to stabilize the Si_{20} fullerene through exohedral decoration with eight Cl substituents and twelve $SiCl_3$ groups on the surface and enclosing Cl^- ion. A deeper understanding on what factors lead to stabilization will open the path for stabilizing other systems of interest. Here, we employ the minima hopping method within density functional theory to understand the potential energy surface. The study shows that the exo-endo halide decoration of the cage alters the glassy nature of the potential energy surface of pure cage to structure seeker. Further analysis of different properties of the global minima, reveal that the extra electron instead of residing on the central encapsulated atom in the cage, it is distributed on the cage and increases the encapsulation energy; thereby stabilizing the system. We also provide estimates of the stability for different kind of exo-endo halide decorations and their feasible realization in experiments.

1 Introduction

The discovery of C_{60} fullerene in 1985 marks an important milestone in nano-sciences¹. Since then, many experimental and theoretical efforts had been made to find fullerene structures made out of non-carbon materials for various applications^{2–4}. Lately, boron based fullerene structure, borospherene B_{40} was discovered by Zhai *et al.* in 2014⁵. As both C and Si both are Group-IV elements without any d orbitals, the Si structures are expected to be similar to their carbon counterparts. Few examples include linear polysilanes, silicon nanosheets and nanotubes^{6–10}.

Since C_{20} forms the smallest known fullerene, Si_{20} clusters were widely studied¹¹. While C atoms can easily adjust their valence states to participate single, double and triple bonds, Si strongly favors sp^3 hybridization in connection with single bonds and this inherent constraint leads to the instability of the Si_{20} fullerene¹².

Endohedral doping of Si_{20} cages with metal atoms, $M@Si_{20}$ was believed for a while to stabilize the cage like geometries. However systematic structure prediction studies show that this strategy fails^{13,14}. The second approach was based on the introduction of exohedral substituents to fully saturate all four sili-

con valencies. The $Si_{20}H_{20}$ dodecahedron configuration has been identified as the global minima^{15,16} in this context. As a third approach, a combination of both techniques was considered which should lead to a stable $M@Si_{20}H_{20}$ where M =metal/halide^{17–19}.

The embedding energy of the endohedral dopants in the hydrogenated cages was found to be smaller than for the bare endohedrally doped fullerene due to weak interaction between the dopant and the cage²⁰. Other than that, such surface passivated endohedrally doped fullerenes proposed in theoretical calculations have very weak interactions among each other and might therefore be stable building blocks for novel materials. It was also predicted that the halide ions, especially Br^- , are ideally suited for the synthesis of $Si_{20}H_{20}$ ¹⁸. However, no such system have been observed in experiments till date.

In our recent study on $Si_{20}H_{20}$ ²¹, we found that its potential energy surface (PES) is complex. The spontaneous formation of $Si_{20}H_{20}$ by condensation is unlikely to occur because the time scale for finding the global minimum is much longer than the time scale for competing processes such as fragmentation or fusion.

Recently, Tillmann *et al.* have developed a one step synthesis protocol by which the Si_{20} dodecahedral core can be stabilized and hence, realized in experiments. The resulting structure is the $[Cl@Si_{32}Cl_{44}]^-$, which consists of a Si_{20} dodecahedral core with an endohedral Cl^- ion and exohedrally decorated with 8 Cl and 12 $SiCl_3$ groups²². Their DFT studies on different possible exohedral decoration with Cl and $SiCl_3$ of the Si_{20} cage structure

^a Department of Physics, Universität Basel, Klingelbergstr. 82, 4056 Basel, Switzerland; E-mail: debsankar.de@unibas.ch; Tel: +41 61 207 3738

^b Institute of Theoretical and Computational Physics, Graz University of Technology, NAWI Graz, 8010 Graz, Austria

provides valuable information about the role of the exohedral decoration on the energetics of the synthesized structure. Later, Vargas et. al.²³ investigated the role of the central halide ion in stabilizing the system based on energy decomposition and multipole analysis.

The study of PES can provide estimate of the synthesizability of a desired compound, the barrier height required to cross and time-scale to synthesize the compound. As explained earlier in Ref.²¹, why it is not feasible to synthesize $\text{Si}_{20}\text{H}_{20}$ and opposite for C_{60} . Thus, the PES is equally important as the properties of the synthesized structure. The two studies Ref.²² and Ref.²³ have focussed primarily on the cage structure of $\text{Cl@Si}_{32}\text{Cl}_{44}$ and the role of either exohedral or endohedral substituents in stabilizing the system. However, the role of the PES in making the synthesis of $[\text{Cl@Si}_{32}\text{Cl}_{44}]^-$ feasible have not been explored yet. Apart from PES, the studies do not address the impact of different combination of exohedral-endohedral decoration of Si_{20} cage and the extra electron in its stabilization.

In this work, the minima hopping method²⁴ was used to explore the potential energy surface(PES) of Si_{20} with different endohedral-exohedral decorations. The runs generated in total 500 distinct structures, which can be classified into fragmented and non-fragmented structures. Distance-energy plots constructed for these structures were used to understand the nature of the PES. In addition, a detailed analysis of the charge density, stability and reactivity of the ground state configuration was conducted. Based on a model of the central halide ion trapped in a spherical potential well, we elucidate the role of exo-endo decorations along with negative charge in the stabilization process.

2 Computational Methodology:

In order to explore the potential energy surface(PES) of the system of interest, the minima hopping method (MHM) was employed^{24,25}. The PES is explored by performing consecutive short molecular dynamics escape steps followed by local geometry relaxations, thereby exploiting the Bell-Evans-Polanyi principle²⁶. The relaxed structures are accepted or rejected based on the threshold set on the energy difference. The transformation pathways were found by the minima hopping guided path search (MHGPS)²⁷.

To identify the structural difference between two configurations and removing the duplicate structures, we have used fingerprint method based on overlap matrix constructed from atom centered Gaussian type orbitals²⁸. More details on the method can be found in the appendix.

All the ab-initio simulation have been performed at the level of density functional theory (DFT) as implemented in BigDFT²⁹. This code uses Daubechies wavelets as a basis set. The atoms were described by the soft Goedecker-type norm-conserving pseudopotentials with non-linear core correction^{30–33} for the Perdew-Burke-Ernzerhof(PBE) exchange correlation functional³⁴. The Libxc library³⁵ coupled with BigDFT was used to evaluate the PBE functionals. A grid spacing of 0.4 Bohr was used. Convergence parameters in BigDFT were set such that total energy differences were converged up to 10^{-4} eV and all configurations were relaxed until the maximal force component on any atom

reached the noise level of the calculation, which was of the order of 1 meV/Å.

The difference in charge density($\Delta\rho$) and electron localization function(ELF)³⁶ was calculated using the VASP code³⁷. The atoms were described by the Projector Augmented Wave potentials as provided in VASP for the PBE functional. In order to mimic the systems under study in free boundary condition, a uniform box of dimension $20 \times 20 \times 20$ Å³ was used. This is the minimum box size required to prevent self interaction between the clusters. For geometric optimization, a energy cut-off of 350 eV was used and for ELF calculation 600 eV.

3 Results and Discussion:

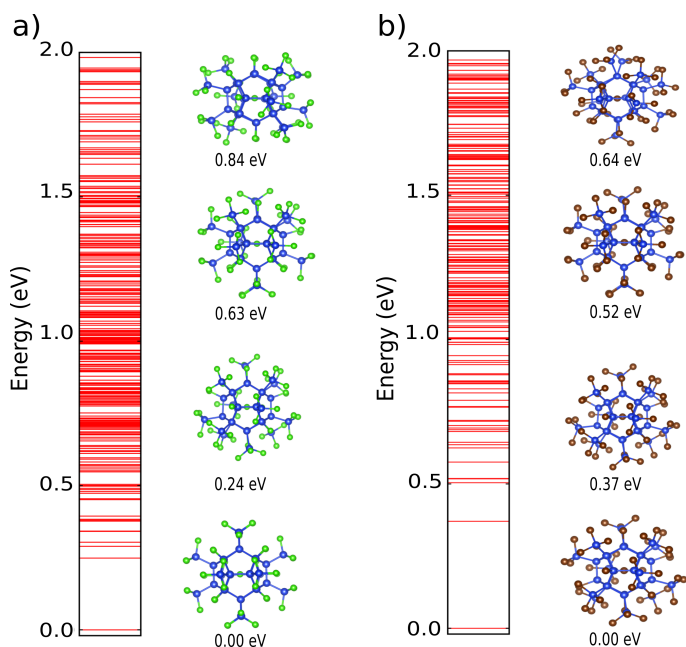


Fig. 1 The configurational energy spectrum of (a) $[\text{Cl@Si}_{32}\text{Cl}_{44}]^-$ and (b) $[\text{Br@Si}_{32}\text{Br}_{44}]^-$, along with the figures of the ground state configuration and next 3 lowest energy structures. The Si, Cl and Br atoms are shown by blue, green and brown sphere, respectively.

3.1 Structure, Geometry and Energetics

A natural starting point of our investigation is the $[\text{Cl@Si}_{32}\text{Cl}_{44}]^-$ symmetric cage structure, experimentally realized by Tillmann et. al.²² in 2015. This $[\text{Cl@Si}_{32}\text{Cl}_{44}]^-$ symmetric structure with D_{2h} symmetry is made of a Si_{20} dodecaheadral core consisting of 20 vertices forming 12 pentagons. Among the 20 vertices, 12 are capped by SiCl_3 groups arranged in pairs and forming the vertices of an octahedron and the remaining 8 are capped with Cl atom. The structure also has an endohedrally doped Cl^- ion. The Si atoms of the cage capped with Cl are represented as Si_0 and SiCl_3 decorated Si as Si_1 .

To rapidly perform an exhaustive configurational search of the PES of $[\text{Cl@Si}_{32}\text{Cl}_{44}]^-$, we carried out MHM runs starting from different configurations; the reported experimental structure and few new configurations were created by exchanging the position of the decorative Cl atoms and SiCl_3 groups. Starting from these

different configurations and after removing the similar structures found in different MHM runs through fingerprint distance, we were left with ~ 500 distinct structures. These structures lie in the energy range $0 \text{ eV} \leq \Delta E \leq 17 \text{ eV}$ w.r.t. the lowest energy structure of $[\text{Cl}@\text{Si}_{32}\text{Cl}_{44}]^-$.

We also carried out investigation on the PES of $[\text{Br}@\text{Si}_{32}\text{Br}_{44}]^-$. The 500 structures obtained for $[\text{Cl}@\text{Si}_{32}\text{Cl}_{44}]^-$ were used as templates for generating structures of $[\text{Br}@\text{Si}_{32}\text{Br}_{44}]^-$ by replacing the Cl atoms with Br and post-relaxing them. As Cl and Br are chemically similar, the $[\text{Br}@\text{Si}_{32}\text{Br}_{44}]^-$ structures easily relaxed without significant distortion and are in the energy range $0 \text{ eV} \leq \Delta E \leq 12 \text{ eV}$ w.r.t. the lowest energy structure of $[\text{Br}@\text{Si}_{32}\text{Br}_{44}]^-$.

The low energy structures generally consist of Si_{20} dodecahedron with diverse arrangement of the Cl and SiCl_3 groups on its vertices. However, the high energy structures consist of mostly fragmented structures along with distorted cage structures. In most cases among the fragmented structures, the SiCl_3 gets fragmented to form a free SiCl_2 with the remaining Cl attached to the Si atom of the cage. This feature of structural motif vs energetic ordering appear to be common in both $[\text{Cl}@\text{Si}_{32}\text{Cl}_{44}]^-$ and $[\text{Br}@\text{Si}_{32}\text{Br}_{44}]^-$.

Based on this two distinct structural motif, the whole structure set can be classified into fragmented and non-fragmented structures. The fragmented structures start to appear at $\Delta E = 1.48 \text{ eV}$ and $\Delta E = 0.96 \text{ eV}$ for $[\text{Cl}@\text{Si}_{32}\text{Cl}_{44}]^-$ and $[\text{Br}@\text{Si}_{32}\text{Br}_{44}]^-$ respectively. Above this energy range, both fragmented and non-fragmented structures can be found. Beyond $\Delta E \geq 4 \text{ eV}$, only the fragmented structures can be found in both $[\text{Cl}@\text{Si}_{32}\text{Cl}_{44}]^-$ and $[\text{Br}@\text{Si}_{32}\text{Br}_{44}]^-$.

The low-energy spectrum of $[\text{Cl}@\text{Si}_{32}\text{Cl}_{44}]^-$ and $[\text{Br}@\text{Si}_{32}\text{Br}_{44}]^-$, which consists of primarily non-fragmented structures is shown in Fig. 1(a) and Fig. 1(b) respectively w.r.t. their corresponding lowest energy structure. Along with this, their 4 lowest energy structures are shown in Fig. 1. Among the predicted $[\text{Cl}@\text{Si}_{32}\text{Cl}_{44}]^-$ clusters, the experimentally observed cage structure with D_{2h} symmetry was found to be the lowest energy structure, where the central Cl^- ion is located at the center of the cage. This theoretical observation also holds true for the $[\text{Br}@\text{Si}_{32}\text{Br}_{44}]^-$ clusters. The distance between the central Cl^- ion and Si from the Si_{20} dodecahedron cage is $\sim 3.28\text{-}3.39 \text{ \AA}$ which is comparable to the experimental values of $3.32\text{-}3.38 \text{ \AA}$. In case of the central Br^- ion in the $[\text{Br}@\text{Si}_{32}\text{Br}_{44}]^-$ cage structure, the distance is $3.31\text{-}3.40 \text{ \AA}$. Thus, the central halide ion to cage distance is similar in both cases.

The other low energy structures have different arrangements of Si_0 and Si_1 on pentagons of the cage. Tillmann et. al.²² through DFT calculation on different decoration of Si_{20} cage with increasing number of SiCl_3 units have found that the ideal arrangement would be that in the pentagon, two consecutive vertices are to be occupied by SiCl_3 units, their immediate neighbouring vertices by Cl atom and the remaining vertices by a SiCl_3 group. Deviation from this symmetric arrangement of Si_1 was found to cost energy of the structures. This is in agreement with our observations.

The second lowest energy isomer of $[\text{Cl}@\text{Si}_{32}\text{Cl}_{44}]^-$ and $[\text{Br}@\text{Si}_{32}\text{Br}_{44}]^-$ are 0.25 eV and 0.37 eV higher than their ground state respectively. This isomer has one non-ideal pentagon con-

sisting of 4 SiCl_3 groups and 1 Cl atoms. The third lowest has two non-ideal pentagons and the fourth lowest with three non-ideal pentagons. Thus, shifting away from the ideal pentagonal arrangement for Cl and SiCl_3 leads to an increase in energy. However, with more non-ideal pentagons, the situation gets complicated as there are many possible decorative arrangements on these pentagons and their relative energetic ordering is not straight forward to understand. At a certain point in high energy spectrum, the cage structure starts to release SiCl_2 with the vertices replaced by Cl atoms. The very high energy structures have completely destroyed cages and free SiCl_4 molecules.

The structures of $[\text{Cl}@\text{Si}_{32}\text{Cl}_{44}]^-$ and $[\text{Br}@\text{Si}_{32}\text{Br}_{44}]^-$ are found to have intermediate to large HOMO-LUMO gaps. Our calculations of 10 lowest energy structures of $[\text{Cl}@\text{Si}_{32}\text{Cl}_{44}]^-$ and $[\text{Br}@\text{Si}_{32}\text{Br}_{44}]^-$ at the level of semilocal DFT are found to be in the range $1.7\text{-}2.0 \text{ eV}$ and $2.0\text{-}2.4 \text{ eV}$ respectively. No specific trends have been found among the HOMO-LUMO gap of different structures. The HOMO-LUMO gaps can be found in the SI.

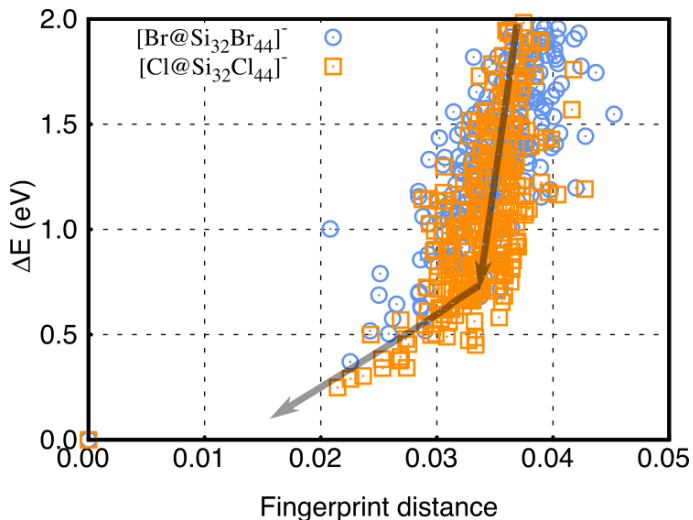


Fig. 2 Distance energy (DE) plot of $[\text{Cl}@\text{Si}_{32}\text{Cl}_{44}]^-$ (open orange square) and $[\text{Br}@\text{Si}_{32}\text{Br}_{44}]^-$ (open blue circle). The energy and the fingerprint distance is w.r.t the lowest energy configuration for each case. For any structure one can find another structure that is more similar to the ground state and that is in nearly all cases lower or in a few cases slightly higher in energy. Hence, one gains quasi continuously energy by moving toward the ground state. The arrow is meant as a guide to the eye, indicating the average driving force.

3.2 Fingerprint Distance-Energy

Apart from the energy ranking of the predicted structures, we also tried to seek insight into the nature of the PES through fingerprint-distance(ΔE) vs energy³⁸ plots. In such a plot, the energy difference(ΔE) is plotted against the fingerprint distance w.r.t. the ground state structure.

The DE plots of both $[\text{Cl}@\text{Si}_{32}\text{Cl}_{44}]^-$ (orange open square) and $[\text{Br}@\text{Si}_{32}\text{Br}_{44}]^-$ (blue open circles) as shown in Fig.7 are found to be similar as the energy separation increases steeply with the increase in fingerprint distance. Their structure seeker character can be easily deduced from the fact that the first few metastable structures are much higher in energy than the ground state, but

not too far in the configurational distance. This suggests that the barrier for jumping from the first metastable structure into the ground state is relatively small and that there is, in general, a strong driving force towards the ground state. The fragmented structures have been removed while constructing the distance-energy plot.

In contrast, the structures of Si_{20} are found to have small ΔE w.r.t. the putative global minima as shown in SI. Details about the generation of Si_{20} structures are provided in the SI. Also, Si_{20} structures with similar energies are found with both small and large fingerprint distance. This points to the fact that one can easily get trapped in one of the local minima and would need to cross barriers of different heights to fall into the global minima. These features are characteristics of a glassy system. This comparative analysis reveals the interesting fact that the exo-endo decoration of Si_{20} not only stabilizes the dodecahedron cage but also alters the PES in such a manner that it changes from glassy to structure seeker.

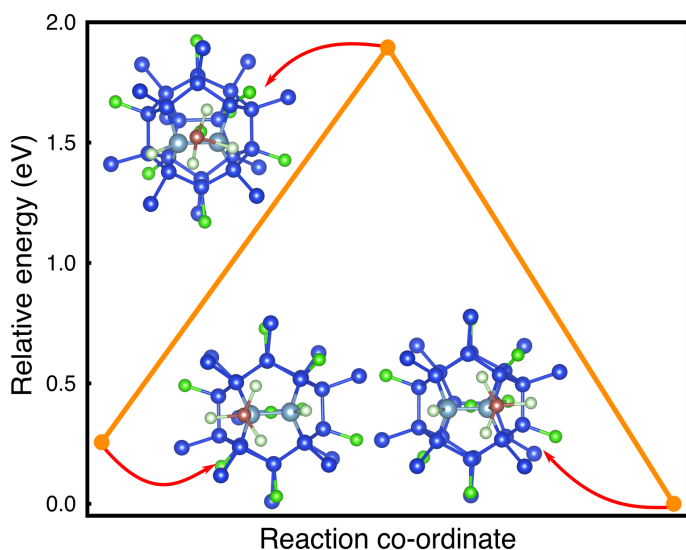


Fig. 3 The transformation path from the first metastable structure of $[\text{Cl}@\text{Si}_{32}\text{Cl}_{44}]^-$ to the $[\text{Cl}@\text{Si}_{32}\text{Cl}_{44}]^-$ ground state. Dark blue sphere represent the Si atoms and light blue, the Si atoms of Si_{20} cage undergoing change in their decoration. The Cl atoms of SiCl_3 are omitted for better visualization. The Si atom of SiCl_3 swapping to another Si atom of Si_{20} cage during the transformation path is shown by pink sphere. Rest all the Cls are by green atoms.

3.3 Transition State

The downhill barrier for transiting from the first metastable state to ground state of $[\text{Cl}@\text{Si}_{32}\text{Cl}_{44}]^-$ is about 1.6 eV as shown in Fig.3. The barrier height is quite high compared to $k_B T$ at room temperature (which corresponds to 0.027 eV). The uphill and downhill barriers are similar with a difference of 0.4 eV. In this process, the SiCl_3 dissociate into SiCl_2 and Cl. The Cl atom stays on top of Si and the SiCl_2 migrates to the nearest Si_0 site and forms SiCl_3 . Standard transition state theory³⁹ gives an attempt frequency of $\omega_A = k_B T / \hbar = 6 \times 10^{12} \text{ sec}^{-1}$ at room temperature. Hence the time required to cross the uphill barrier is 10^{15} sec at room temperature.

In order to assess the possibility and reaction time at higher temperature, we estimated the Boltzmann probabilities as a function of temperature for the 10 lowest energy structures of $[\text{Cl}@\text{Si}_{32}\text{Cl}_{44}]^-$ and $[\text{Br}@\text{Si}_{32}\text{Br}_{44}]^-$. The details of the calculation of the Boltzmann probability plot and the figure (Fig. 1 in appendix) is provided in appendix. The Boltzmann probabilities show that the ground state structure of $[\text{Br}@\text{Si}_{32}\text{Br}_{44}]^-$ is dominant until $\sim 1200 \text{ K}$ and for $[\text{Cl}@\text{Si}_{32}\text{Cl}_{44}]^-$ until $\sim 800 \text{ K}$. At higher temperatures, other low energy structures start to emerge.

Hence, considering 800 K as the upper limit, the time required for transition at 800 K is around 0.2 msec. Since, the experimental synthesis was carried out in a solvent medium the actual barrier height could be considerably lower than our calculated height.

3.4 Bonding and ELF Analysis

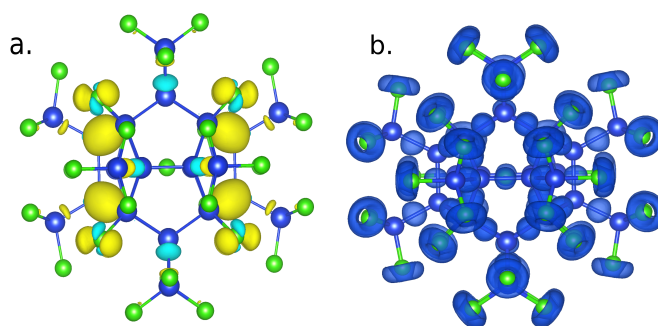


Fig. 4 a) Charge density difference between neutral and charged $\text{Cl}@\text{Si}_{32}\text{Cl}_{44}$. b) ELF of $[\text{Cl}@\text{Si}_{32}\text{Cl}_{44}]^-$ at $\eta=0.88$. The Si and Cl atoms are shown by blue and green sphere, respectively.

In order to investigate where the extra electron added to the $[\text{Cl}@\text{Si}_{32}\text{Cl}_{44}]^-$ is localized, the $\Delta\rho$ between the $[\text{Cl}@\text{Si}_{32}\text{Cl}_{44}]^-$ and $[\text{Cl}@\text{Si}_{32}\text{Cl}_{44}]$ is shown in Fig 4(a) where, the yellow colour indicates the presence of extra electronic charge and blue electronic deficiency. The plot shows that when an electron is added, it doesn't reside on the central Cl atom. Rather, the Si as well as Cl atoms of the Si_0 decoration on the cage gain some electronic charge at the expense of losing electronic charge from Si atoms with Si_1 decoration. There is no significant difference in the charge density of the Cl in the SiCl_3 groups in Si_1 decoration.

The ELF of $[\text{Cl}@\text{Si}_{32}\text{Cl}_{44}]^-$ at isosurface value of 0.88 is shown in Fig 4(b). The circular lobes on the Cl atoms indicate the presence of lone pair electrons on them.

3.5 Dissociation and Coalescence

The analysis carried out above on the PES and on ground state configuration of $[\text{Cl}@\text{Si}_{32}\text{Cl}_{44}]^-$ doesn't necessarily shed light on its reactivity. In order to understand its reactive/inert nature, we accessed if it is stable against dissociation or coalescence.

Fragmentation of $[\text{Cl}@\text{Si}_{32}\text{Cl}_{44}]^-$ has been observed in the laser-desorption ionization(LDI) MS(-) experiments²². As mentioned earlier, the SiCl_3 group fragments to form a free SiCl_2 molecule and the remaining Cl atom gets adsorbed on the Si atom of the Si_{20} cage. A major fragmentation cascade is observed due

to the extrusions of such SiCl_2 groups. Similar structures also were found in our MHM search. Through our DFT calculation, we found that the ground state configuration is found to be local minimum and stable under dissociation of one SiCl_2 and two SiCl_2 groups with dissociation energy 1.49 and 2.70 eV, respectively. The dissociation energy is defined as the difference between the cluster and the individual components of the fragmented parts of the cluster under vacuum condition.

The issue of coalescence of the ground minimum of $[\text{Cl@Si}_{32}\text{Cl}_{44}]^-$ and $[\text{Br@Si}_{32}\text{Br}_{44}]^-$ was addressed by estimating the energy required to form dimers. The dimers were created by bringing the ground state configuration in proximity for three different relative orientation (see appendix) and relaxing them without any constraint. It turns out that both the $[\text{Cl@Si}_{32}\text{Cl}_{44}]^-$ and $[\text{Br@Si}_{32}\text{Br}_{44}]^-$ are chemically inert and repel each other, as indicated by their positive binding energy of dimer. The binding energy of the dimer is defined as the difference between the energy of the dimer and the energy of the monomers. The factor leading to repulsion is the presence of lone pair electrons on peripheral Cl atoms as shown in ELF analysis (Fig. 4).

3.6 Exohedral and Endohedral Substituents

The complex dependency of different exohedral and endohedral decorations along with the extra electron in stabilizing the Si_{20} cage makes their understanding challenging. Vargas et. al.²³ through energy decomposition analysis tried to decipher the role of substituents and suggested alternative halide based substituents which can stabilize the cage. Though such analysis are useful, they are complicated and often not easy to decipher.

The central halide ion in the cage can be considered to be a particle trapped in a spherical potential well. Considering this simple picture, one can easily assimilate the combined effect of the exohedral/endohedral substituents and the additional electron to a single quantity i.e., the curvature of the potential.

For our tests we considered $[\text{Cl@Si}_{32}\text{Cl}_{44}]^{-1}$, $[\text{Cl@Si}_{32}\text{Cl}_{44}]$, $[\text{Br@Si}_{32}\text{Cl}_{44}]^{-1}$, $[\text{Cl@Si}_{20}\text{H}_{20}]^{-1}$ and $[\text{Br@Si}_{32}\text{Br}_{44}]^{-1}$ cases. The radius of the cage is different for different decorations. The change in energy $\Delta E(\text{eV})$ w.r.t. displacement (\AA) of the central atom of the cage shows that the potential of the charged and neutral case are on top of each other for all the systems, giving clear indication that the extra electron on the structure does not effect the stability of the center atom (see appendix). The curvature of the systems with central Br ion is larger than the ones with central Cl ion. This is due to the large ionic radius of Br as compared to Cl confined in the cage structure of similar diameter. The large ionic radius leads to steep increase in potential w.r.t. displacement. Hence, the potential is influenced by the substituents and not by the extra electron.

As evident from above, the spring constant K of the potential for $[\text{Cl@Si}_{32}\text{Cl}_{44}]$ remains approximately same for both the neutral and charged system. However, the encapsulation energy (E.E.) increases by factor of ~ 1.84 for charged system as compared to neutral case. The extra stabilization due to addition of an electron is also supported by the large electron affinity. This behavior holds true for other endo-exo decoration of Si_{20} dodecahedron

considered. The electron affinity depends only on the exohedral substituents. The values for different decorations are provided in the SI. Thus, the extra electron doesn't lead to increase in interaction between the central atom and the cage, rather goes to the cage and stabilizes it.

4 Conclusion

In conclusion, through exploration of the PES of $[\text{Cl@Si}_{32}\text{Cl}_{44}]^-$ and $[\text{Br@Si}_{32}\text{Br}_{44}]^-$, we found that the experimentally observed symmetric cage structure is the putative global minima. The exo-endo decoration of Si_{20} cage with Cl and SiCl_3 transforms the nature of PES from glassy to structure seeker. At room temperature the symmetric cage structure is the most viable isomer during synthesis. However, at higher temperature, other isomers would start to emerge. The ground state minimum is stable against dissociation and coalescence. Our stability analysis suggests that the experimental efforts could be oriented towards the synthesis of the hypothetical counterpart $[\text{Br@Si}_{32}\text{Br}_{44}]^-$ of $[\text{Cl@Si}_{32}\text{Cl}_{44}]^-$.

The $\Delta\rho$ shown in Fig.4 coupled with the central atom displacement study modeled into a particle trapped in a spherical potential well clearly indicate that the extra electron instead of residing on the central halide atom, gets distributed on the cage and stabilizes it by increasing the inter-atomic interaction within the cage, rather between the central atom and the cage. As a result of this, the extra electron leads to significant increase in encapsulation energy, thereby making the combined system more stable.

Conflicts of interest

There are no conflicts to declare.

Acknowledgements

D.S.D acknowledge support from the Swiss National Science Foundation. Computational resources provided by the Swiss National Supercomputing Center (CSCS) in Lugano under the projects s707 and s963 are gratefully acknowledged. Calculations were also performed at the sciCORE (<http://scicore.unibas.ch/>) scientific computing core facility at the University of Basel. This was supported by the NCCR MARVEL, funded by the Swiss National Science Foundation.

A Finger print method:

The configurational fingerprints are given by the eigenvalues of an overlap matrix O .

$$O_{ij} = \int \phi_i^l(r) \phi_j^{l'}(r) dr \quad (1)$$

where ϕ_i are the Gaussian type orbitals centered on the atom at position r_i and is given by

$$\phi_i^l(r) \propto (x-x_i)^{l_x} (y-y_i)^{l_y} (z-z_i)^{l_z} \exp(-\alpha_i |r-r_i|^2) \quad (2)$$

Here $l=(l_x, l_y, l_z)$ is an angular momentum $L=l_x+l_y+l_z$. The orbitals are classified depending on their value of L i.e. s -type orbital is $L=0$, p -type orbital is $L=1$, or d -type orbital is $L=3$. α_i is the orbital width and they are inversely proportional to the covalent radius of the atoms on which the orbitals are centered on. The structural difference is given by the root mean square difference of the two fingerprint vectors. This fingerprint distance is invariant under translations, rotations, reflections as well as under the permutation of the atomic indices.

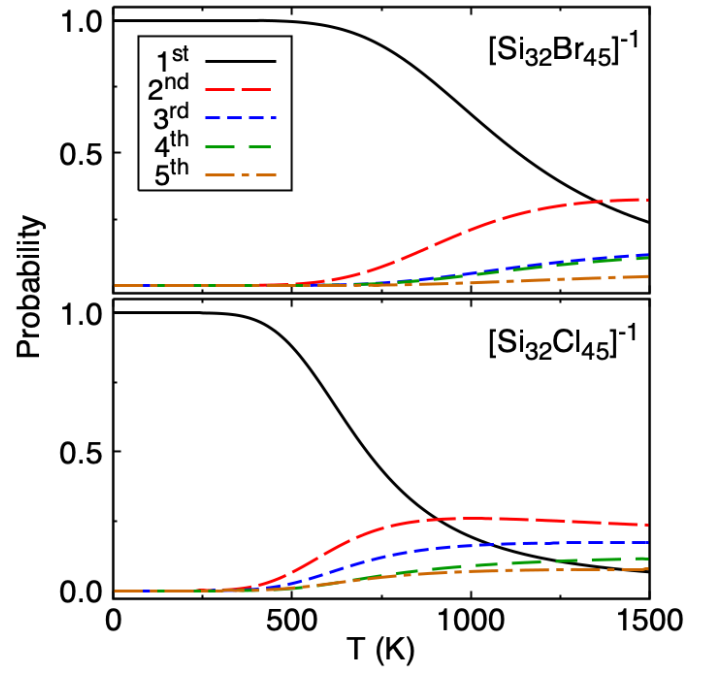


Fig. 5 The Boltzmann probability distribution of 5 lowest energy structures of [Cl@Si₃₂Cl₄₄]⁻ (bottom panel) and The Boltzmann probability have been estimated for 10 lowest energy structures.

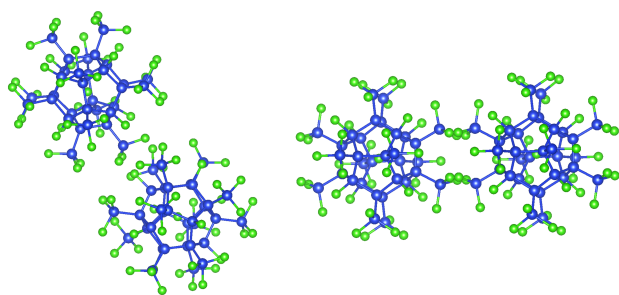


Fig. 6 Dimers are constructed by adding two GS configurations along X, Z and X-Y directions. Here we show the structures which are formed by adding the GS configurations along X and X-Y direction.

System	Gap in Angstroem
$\text{Si}_{32}\text{Cl}_{45}^-$	6.736
$\text{Si}_{32}\text{Cl}_{45}$	6.787
$\text{Si}_{32}\text{Cl}_{44}\text{Br}^-$	6.749
$\text{Si}_{32}\text{Br}_{45}^-$	6.679
$\text{Si}_{20}\text{H}_{20}\text{Cl}^-$	6.629

Table 1 Diameter of the gap in the X-Y plane.

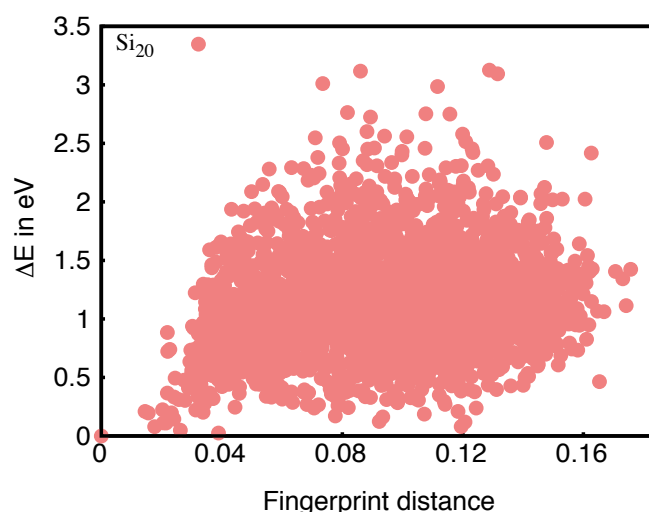


Fig. 7 Distance Energy (DE) plot of Si_{20} clusters. The finger print distances and energy differences are calculated with respect to the ground state configuration. There is no driving force towards the ground state.

B Exohedral and Endohedral Substituents

Based on this simplistic picture of a particle trapped in a 1D-potential, we estimated the spring constant of the quadratic potential. The potential can be easily constructed by obtaining the energy difference as a function of displacement, where the reference energy is the energy of the geometrically relaxed structure. During the displacement of the central atom, the whole structure is kept fixed and only scf runs were done to obtain the total energy. In addition we also calculated encapsulation energy (E.E.) and electron affinity (E.A.). Encapsulation energy is given by:

$$\text{E.E.} = E_{\text{system}} - E_{\text{cage}} - E_{\text{central atom}} \quad (3)$$

where E_{system} is the energy of the whole system cage + center anion(neutral or charged), E_{cage} energy of the empty cage without the central atom and $E_{central\ anion}$ energy of the central halogen (neutral or charged state). Electron affinity (E.A.) is given by

$$E.A. = E_{neutral\ system} - E_{charged\ system} \tag{4}$$

where $E_{charged\ system}$ is the energy of the charged cage and $E_{neutral\ system}$ is the energy of the charged cage.

The E.E., spring constant K and E.A. of these systems are listed in Table.2. As seen above in the Fig.8 and also from the K values, they are similar for charged and neutral states. The E.E. sheds light on the role of the extra electron, i.e. it reduces the total energy, making it more stable and is also supported by the large E.A. Its also interesting to note that the E.A. is not effected by the type of central halide ion, but rather by the exohedral decoration.

Table 2 Encapsulation Energy (eV), Harmonic oscillator strength K (eV/Å²) and electron affinity E.A.(eV) for different decorations of Si₂₀ do-decahedron.

System	E.E. (eV)		K (eV/Å ²)		E.A. (eV)
	Neutral	Charge	Neutral	Charge	
Cl@Si ₃₂ Cl ₄₄	-2.34	-4.38	2.16	2.08(X,Y,Z)	5.68
Br@Si ₃₂ Cl ₄₄	-1.87	-4.15	2.91	2.82	5.68
Cl@Si ₃₂ Br ₄₄	-2.48	-4.28	1.89	1.90	5.43
Br@Si ₃₂ Br ₄₄	-2.03	-4.07	2.62	2.60	5.44
Cl@Si ₂₀ H ₂₀	-0.07	-0.10	2.70	2.69	0.16
Br@Si ₂₀ H ₂₀	-0.05	-0.09	3.82	3.81	0.16

Notes and references

- 1 H. W. Kroto, J. R. Heath, S. C. O'Brien, R. F. Curl and R. E. Smalley, *nature*, 1985, **318**, 162–163.
- 2 W. Song, C. Querebillo, R. Götz, S. Katz, U. Kuhlmann, U. Gernert, I. Weidinger and P. Hildebrandt, *Nanoscale*, 2017, **9**, 8380–8387.
- 3 Z. Yang, Y.-L. Ji, G. Lan, L.-C. Xu, X. Liu and B. Xu, *Solid State Communications*, 2015, **217**, 38–42.
- 4 M. P. Johansson, D. Sundholm and J. Vaara, *Angewandte Chemie*, 2004, **116**, 2732–2735.
- 5 H.-J. Zhai, Y.-F. Zhao, W.-L. Li, Q. Chen, H. Bai, H.-S. Hu, Z. A. Piazza, W.-J. Tian, H.-G. Lu, Y.-B. Wu *et al.*, *Nature chemistry*, 2014, **6**, 727–731.
- 6 H. W. Gibson, R. J. Weagley, R. A. Mosher, S. Kaplan, W. M. Prest and A. J. Epstein, *Phys. Rev. B*, 1985, **31**, 2338–2342.
- 7 K. S. Novoselov, A. K. Geim, S. V. Morozov, D. Jiang, M. I. Katsnelson, I. V. Grigorieva, S. V. Dubonos and A. A. Firsov, *Nature*, 2005, **438**, 197–200.
- 8 P. Boul, J. Liu, E. Mickelson, C. Huffman, L. Ericson, I. Chiang, K. Smith, D. Colbert, R. Hauge, J. Margrave and R. Smalley, *Chemical Physics Letters*, 1999, **310**, 367–372.
- 9 R. D. Miller and J. Michl, *Chemical Reviews*, 1989, **89**, 1359–1410.
- 10 H. Okamoto, Y. Kumai, Y. Sugiyama, T. Mitsuoka, K. Nakanishi, T. Ohta, H. Nozaki, S. Yamaguchi, S. Shirai and H. Nakano, *Journal of the American Chemical Society*, 2010, **132**, 2710–2718.
- 11 B.-x. Li and P.-l. Cao, *Physical Review A*, 2000, **62**, 023201.
- 12 K.-M. Ho, A. A. Shvartsburg, B. Pan, Z.-Y. Lu, C.-Z. Wang, J. G. Wacker, J. L. Fye and M. F. Jarrold, *Nature*, 1998, **392**, 582–585.
- 13 A. Willand, M. Gramzow, S. A. Ghasemi, L. Genovese, T. Deutsch, K. Reuter and S. Goedecker, *Physical Review B*, 2010, **81**, 201405.
- 14 Q. Sun, Q. Wang, T. Briere, V. Kumar, Y. Kawazoe and P. Jena, *Physical Review B*, 2002, **65**, 235417.
- 15 C. W. Earley, *The Journal of Physical Chemistry A*, 2000, **104**, 6622–6627.
- 16 A. D. Zdetsis, *Physical Review B*, 2007, **76**, 075402.
- 17 C.-Y. Zhang, H.-S. Wu and H. Jiao, *Chemical physics letters*, 2005, **410**, 457–461.
- 18 F. Pichierri, V. Kumar and Y. Kawazoe, *Chemical physics letters*, 2005, **406**, 341–344.
- 19 D. Palagin and K. Reuter, *Physical Review B*, 2012, **86**, 045416.
- 20 V. Kumar and Y. Kawazoe, *Physical Review B*, 2007, **75**, 155425.
- 21 D. S. De, B. Schaefer, B. von Issendorff and S. Goedecker, *Physical Review B*, 2020, **101**, 214303.
- 22 J. Tillmann, J. H. Wender, U. Bahr, M. Bolte, H.-W. Lerner, M. C. Holthausen and M. Wagner, *Angewandte Chemie*, 2015, **127**, 5519–5523.
- 23 M. Ponce-Vargas and A. Muñoz Castro, *The Journal of Physical Chemistry C*, 2018, **122**, 12551–12558.
- 24 S. Goedecker, *The Journal of chemical physics*, 2004, **120**, 9911–9917.
- 25 B. Schaefer, S. A. Ghasemi, S. Roy and S. Goedecker, *The Journal of chemical physics*, 2015, **142**, 034112.
- 26 S. Roy, S. Goedecker and V. Hellmann, *Physical Review E*, 2008, **77**, 056707.
- 27 B. Schaefer, S. Mohr, M. Amsler and S. Goedecker, *The Journal of chemical physics*, 2014, **140**, 214102.
- 28 A. Sadeghi, S. A. Ghasemi, B. Schaefer, S. Mohr, M. A. Lill and S. Goedecker, *The Journal of chemical physics*, 2013, **139**, 184118.
- 29 L. Genovese, A. Neelov, S. Goedecker, T. Deutsch, S. A. Ghasemi, A. Willand, D. Caliste, O. Zilberberg, M. Rayson, A. Bergman *et al.*, *The Journal of chemical physics*, 2008, **129**, 014109.
- 30 C. Hartwigsen, S. Goedecker and J. Hutter, *Physical Review B*, 1998, **58**, 3641.
- 31 S. Goedecker, M. Teter and J. Hutter, *Physical Review B*, 1996, **54**, 1703.
- 32 M. Krack, *Theoretical Chemistry Accounts*, 2005, **114**, 145–152.
- 33 A. Willand, Y. O. Kvashnin, L. Genovese, Á. Vázquez-Mayagoitia, A. K. Deb, A. Sadeghi, T. Deutsch and S. Goedecker, *The Journal of chemical physics*, 2013, **138**, 104109.
- 34 J. P. Perdew, K. Burke and M. Ernzerhof, *Physical review letters*, 1996, **77**, 3865.
- 35 M. A. Marques, M. J. Oliveira and T. Burnus, *Computer physics communications*, 2012, **183**, 2272–2281.
- 36 B. Silvi, A. Savin *et al.*, *Nature*, 1994, **371**, 683–686.
- 37 G. Kresse and J. Furthmüller, *Physical review B*, 1996, **54**, 11169.
- 38 S. De, B. Schaefer, A. Sadeghi, M. Sicher, D. G. Kanhere and S. Goedecker, *Phys. Rev. Lett.*, 2014, **112**, 083401.
- 39 H. Eyring, *The Journal of Chemical Physics*, 1935, **3**, 107–115.

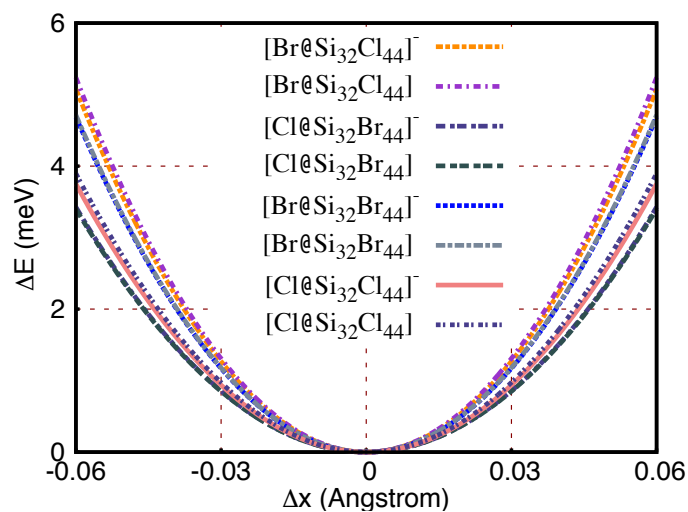


Fig. 8 Change in total energy ΔE (eV) as a function of displacement (Δx) in Å of the center atom for different combination of exohedral and endohedral decoration in the Si_{20} dodecahedron cage. The reference energy for each case was the total energy of the ground state structure and the reference length for the displacement was the radius of the cage for corresponding decoration. The cage structure was kept fixed during the displacement of the center atom.